Electronic Spectrum of AuF: Hyperfine Structure of the [17.7]1 State†

Benjamin J. Knurr, Elissa K. Butler, and Thomas D. Varberg*

Department of Chemistry, Macalester College, 1600 Grand Avenue, St. Paul, Minnesota 55105

Received: May 13, 2009; Revised Manuscript Received: June 10, 2009

The $[17.7]1-X^1\Sigma^+$ (0,0) band of AuF at 566 nm has been studied by laser excitation spectroscopy. The molecule was prepared in a dc electric discharge by flowing a dilute mixture of SF_6 in argon through a hollow gold cathode. The rotational structure of the band has been analyzed for the first time, yielding accurate values for the rotational and Ω-type doubling constants of the upper state. Hyperfine splittings arising from both the ^{197}Au and ^{19}F nuclei have been resolved by recording the spectrum at sub-Doppler resolution using the technique of intermodulated fluorescence spectroscopy. The hyperfine structure is dominated by the ^{197}Au magnetic dipole interaction in the [17.7]1 state, with the ^{197}Au magnetic hyperfine constant determined to be $h_1 = -543(4)$ MHz. It is demonstrated that the negative value of this constant implies that the [17.7]1 state has significant $^3\Delta_1$ character and that spin−orbit mixing with a $^1\Pi_1$ state may be providing the transition intensity to the ground electronic state.

Introduction

There has been a number of studies on the spectroscopy of the molecule gold monofluoride (AuF). The first experimental report of a spectrum of gaseous AuF appeared in 1992 when Saenger and Sun[1] described emission bands in the yellow region, recorded with a resolution of 0.2 nm. They identified several vibrational bands with $\Delta v = 0$ and -1 of an electronic system tentatively assigned as $^1\Pi-^1\Sigma$. Later, Andreev and BelBruno[2] recorded these same bands at a resolution that was still not high enough to permit a rotational analysis. They recorded several $\Delta v = 0$ and ± 1 vibrational bands and found that they corresponded to two closely spaced electronic transitions. They assigned these two transitions as $^1\Sigma^+-X^1\Sigma^+$ and $^1\Pi-X^1\Sigma^+$, guided by calculations using density functional theory.

The ground state of AuF has been the subject of two high-resolution studies. Using Fourier transform microwave spectroscopy, Evans and Gerry[3] recorded the $J = 1$ to 0 rotational transition in the $v = 0$ and 1 levels of the $X^1\Sigma^+$ state, determining accurate values for the rotational, electric quadrupole, and nuclear spin-rotation constants. Okabayashi et al.[4] extended this measurement of the pure rotational spectrum to $v'' = 13$ and $J'' = 27$ using a source-modulated microwave spectrometer. They performed a least-squares fit to all measured transitions using a Dunham-type expansion, determining rotational and vibrational constants for the ground state. Several computational studies of the AuF molecule have also been reported, two of which have included excited electronic states.[5,6]

Our interest in the molecule stemmed from a desire to undertake a rotational and hyperfine analysis of the previously reported but unassigned electronic bands in the yellow region and also to search for other transitions in the visible region. We have succeeded in recording spectra of the (0,0), (1,1), (0,1), and (1,1) bands of the two states in the yellow region at rotational resolution. We have also observed two weaker bands at 688 and 715 nm, which we have tentatively identified as the (1,0) and (0,0) bands of a $\Omega' = 1-X^1\Sigma^+$ transition.

The upper states in the yellow bands, [17.8]0 and [17.7]1, lie only 102 cm^{-1} apart. In labeling these states, we use the Hund's case c notation first described by Linton et al.:[7] $[T_0]\Omega$, where T_0 is the energy of the state in 10^3 cm^{-1}, relative to $X^1\Sigma^+$ ($v = 0$). The two upper states could potentially be assigned as $^1\Sigma^+$ and $^1\Pi$ states, as previously reported,[1,2] or as components of a $^3\Sigma^-$ state. In fact, as Steimle et al.[8] have shown, these two models are isomorphic and will equivalently describe the rotational, fine, and hyperfine structures. In either case, we anticipate large spin−orbit mixing of the excited electronic states of AuF, so that these case a designations indicate only the leading character of the upper states. We also considered the possibility that the [17.7]1 state is a $^3\Pi_1$ state, as indicated in the ab initio study.[6] However, in fitting the ^{197}Au hyperfine structure of the band, we have found that the sign of the case c magnetic hyperfine constant h_Ω of the upper state is negative: $h_1 = -543(4)$ MHz. A negative value for this constant is inconsistent with the upper state being pure $^1\Pi_1$, $^3\Sigma^-$, or $^3\Pi_1$. As we will show, the only Hund's case a singlet or triplet state capable of producing a negative h_1 constant is $^3\Delta_1$. Therefore, the [17.7]1 state must have significant $^3\Delta_1$ character, with electric dipole transition intensity to the ground $^1\Sigma^+$ state provided by a large spin−orbit interaction with a $^1\Pi_1$ state that is calculated to lie in the same energy region.[6] In this article, we will describe our analysis of the hyperfine structure of the $[17.7]1-X^1\Sigma^+$ (0,0) band at 566 nm. We will report elsewhere on the vibrational and rotational structure of the yellow and red systems of AuF.

Experimental Methods

We recorded the visible spectrum of gold fluoride (AuF) by laser excitation spectroscopy using a hollow cathode sputtering source to generate the molecules. Argon with a trace amount of sulfur hexafluoride (SF_6) was flowed through a 3 mm diameter hole in a 6 mm diameter, 10 mm long solid gold cathode. A wire anode was placed 10 mm from the cathode, and a 7 mA dc electric discharge was struck and maintained. The resulting plasma was expanded downward through a 3 mm wide slit into a chamber pumped to approximately 1.6 Torr. The laser beam entered the chamber horizontally, crossing

† Part of the "Robert W. Field Festschrift".

* To whom correspondence should be addressed. E-mail: varberg@macalester.edu. Tel: 651-696-6468. Fax: 651-696-6432.

10.1021/jp904472y CCC: $40.75
Published on Web 07/06/2009

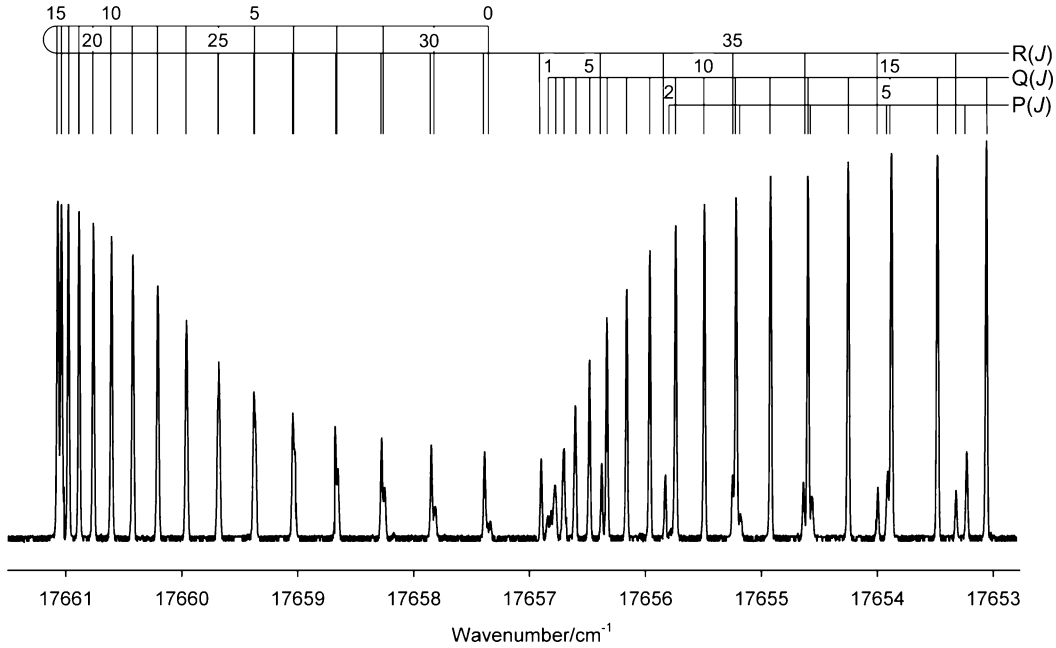

Figure 1. Portion of the [17.7]1−$X^1\Sigma^+$ (0,0) band of AuF recorded at Doppler-limited resolution.

through molecular flow 10 mm below the slit. Molecular fluorescence was collected at *f*/2 by a 50 mm diameter lens and passed through a colored glass filter that transmitted light of the excitation wavelength and longer. This filter blocked bluer emission from the argon discharge, thus improving the signal-to-noise ratio. The fluorescence was then focused onto a side-on photomultiplier tube (Hamamatsu R928).

We began our studies of AuF by recording spectra with a pulsed dye laser. With a resolution of ∼0.1 cm^{-1}, we were not able to resolve fully the rotational structure with this laser, but we could rapidly scan wide spectral regions to identify electronic bands of interest. We recorded high-resolution spectra using a single-mode, continuous-wave ring laser (Coherent 899-29 pumped by a Coherent Verdi V-10 laser) operating with Rhodamine 6G dye as the lasing medium. The laser radiation was mechanically chopped, and the fluorescence signal was demodulated with a lock-in amplifier (Stanford SR510). The laser bandwidth was less than 1 MHz so that the molecular line width of ∼450 MHz (fwhm) was governed by Doppler broadening.

To resolve the hyperfine structure, we recorded many rotational lines at sub-Doppler resolution using intermodulated fluorescence spectroscopy.[9] In this method, we split the laser radiation into two beams of equal intensity with a beam splitter, chopped each beam at a different frequency, and counter-propagated the two beams nearly collinearly through the center of the molecular flow. The power in each beam was reduced to 25 mW to provide the best compromise between narrowing the (power-broadened) line width and improving the signal-to-noise ratio. The sum of the two chopping frequencies was used as the lock-in reference frequency to record Lamb dips without a Doppler-limited background. The frequency scan rate was 5 MHz/s with a lock-in time constant of 1 s. Under these conditions, the line width of the narrowest sub-Doppler features was about 30 MHz (fwhm). We calibrated the ring laser's wavemeter absolutely by recording optogalvanic spectra of atomic argon using an Nb metal hollow cathode lamp filled with argon. We estimate that the relative measurement uncertainty of strong sub-Doppler features across the whole band is approximately ±0.001 cm^{-1}, whereas the absolute uncertainty is about ±0.005 cm^{-1}.

Results

Armed with accurate combination differences for the ground state from the microwave work,[3,4] the assignment of the rotational structure of the band was straightforward. A portion of the spectrum near the origin is shown in Figure 1. The values of the rotational and centrifugal distortion constants are such that pairs of outgoing and returning R lines coincide over the range $J = 0$ to 31. However, for each of the first several R lines, the separation from a returning high-J R line is great enough that there was no blending in the sub-Doppler spectra. The first lines in the three branches are R(0), Q(1), and P(2), and the unambiguous absence of a P(1) line, verified by the sub-Doppler measurements, definitively identifies the upper state as $\Omega' = 1$. There is significant Ω-type doubling in the upper state, with a splitting that increases as J^2, as one expects for an $\Omega = 1$ state.[10]

A close inspection of the first few lines in each of the three rotational branches revealed unresolved hyperfine structure in the Doppler-limited spectrum. To analyze this structure, we recorded intermodulated fluorescence spectra of a total of 16 rotational lines for which the hyperfine components were unblended at our sub-Doppler resolution. The [17.8]0−$X^1\Sigma^+$ (0,0) band, by contrast, showed no perceptible broadening at Doppler-limited resolution, and sub-Doppler spectra of several different lines in this band revealed no resolvable hyperfine structure.

The large spin−orbit interactions in a gold-containing molecule such as AuF will strongly mix the various Hund's case a states. With this in mind, we chose to write our Hamiltonian in a Hund's case c basis for the [17.7]1 state. For both the upper and ground states, the rotational and centrifugal distortion terms were written as

$$\langle J\Omega|\mathbf{H}_{\mathrm{rot}}|J\Omega\rangle = BJ(J+1) - DJ^2(J+1)^2 + HJ^3(J+1)^3 \quad (1)$$

We treated the Ω-type doubling in the [17.7]1 state using the matrix elements

$$\langle J\Omega_f^e|\mathbf{H}_{\text{o.d.}}|J\Omega_f^e\rangle = \pm\frac{1}{2}[qJ(J+1) + q_D J^2(J+1)^2 + q_H J^3(J+1)^3] \quad (2)$$

With this Hamiltonian, we did an initial fit of the three rotational branches of the [17.7]1−$X^1\Sigma^+$ (0,0) Doppler-limited spectrum up to $J \approx 50$, which provided good estimates of the molecular constants. Presumably, the [17.8]0 state only 102 cm^{-1} away is the primary contributor to the Ω-doubling of the [17.7]1 state. The effective Hamiltonian described by eqs 2 and 3 was adequate for fitting the rotational structure of the [17.7]1−$X^1\Sigma^+$ transition within the experimental uncertainty. The values of the centrifugal distortion constants (rotational and Ω-doubling) were subsequently used as fixed constants in our least-squares fit to the low-J hyperfine-resolved lines recorded at sub-Doppler resolution.

To fit the hyperfine structure, we developed the appropriate hyperfine Hamiltonian to treat the two electronic states. Gold and fluorine each exist as single isotopes with nuclear spin: ^{197}Au, $I = 3/2$, and ^{19}F, $I = 1/2$. In our basis set, we coupled the nuclear spin momenta in the order $\mathbf{J} + \mathbf{I_1}$ (^{197}Au) $= \mathbf{F_1}$; $\mathbf{F_1} + \mathbf{I_2}$ (^{19}F) $= \mathbf{F}$. We anticipated that the hyperfine structure arises from ^{197}Au and ^{19}F magnetic dipole and ^{197}Au electric quadrupole interactions. Matrix elements of the hyperfine Hamiltonian evaluated in a case a_β basis are available in the literature for the first[11] and second[12] nucleus of a two-spin diatomic molecule. These matrix elements can be expressed in a case c_β basis by evaluating those elements that are diagonal in Ω (that is, by setting $\Sigma = \Sigma'$), with the case c magnetic hyperfine parameter, h_Ω, defined as a linear combination of case a parameters: $h_\Omega = a\Lambda + (b_F + (2/3)c)\Sigma$. (See the Discussion section.) Therefore, for a case c Ω-component, there is only one parameter determinable from the magnetic hyperfine structure for each nucleus, $h_\Omega^{(1)}$ (^{197}Au) and $h_\Omega^{(2)}$ (^{19}F). These hyperfine matrix elements are as follows

$$\begin{aligned}\langle J\Omega I_1F_1I_2F|\mathbf{H}_{\text{mag}}|J'\Omega I_1F'_1I_2F\rangle = (&h_\Omega^{(1)}(-1)^{J'+I_1+F_1} \times \\ &[I_1(I_1+1)(2I_1+1)]^{1/2}\begin{Bmatrix} I_1 & J' & F_1 \\ J & I_1 & 1\end{Bmatrix}\delta_{F_1F'_1} + \\ &h_\Omega^{(2)}(-1)^{J+I_1+I_2+2F'_1+F+1}[I_2(I_2+1)(2I_2+1)]^{1/2} \times \\ &[(2F_1+1)(2F'_1+1)]^{1/2}\begin{Bmatrix} I_2 & F'_1 & F \\ F_1 & I_2 & 1\end{Bmatrix}\begin{Bmatrix} J' & F'_1 & I_1 \\ F_1 & J & 1\end{Bmatrix}) \times \\ &[(2J+1)(2J'+1)]^{1/2}(-1)^{J-\Omega}\begin{pmatrix} J & 1 & J' \\ -\Omega & 0 & \Omega\end{pmatrix}\end{aligned} \quad (3)$$

and

$$\begin{aligned}\langle J\Omega I_1F_1I_2F_f^e|\mathbf{H}_{\text{elec}}|J'\Omega I_1F'_1I_2F_f^e\rangle = &\left(\frac{1}{4}eQq_0^{(1)}\begin{pmatrix} J & 2 & J' \\ -\Omega & 0 & \Omega\end{pmatrix} \pm \frac{1}{4\sqrt{6}}eQq_2^{(1)}\begin{pmatrix} J & 2 & J' \\ -\Omega & 2 & -\Omega\end{pmatrix}\right) \times \\ &(-1)^{J'+I_1+F_1+J-\Omega}[(2J+1)(2J'+1)]^{1/2}\begin{Bmatrix} I_1 & J' & F_1 \\ J & I_1 & 2\end{Bmatrix} \times \\ &\begin{pmatrix} I_1 & 2 & I_1 \\ -I_1 & 0 & I_1\end{pmatrix}^{-1}\delta_{F_1F'_1}\end{aligned} \quad (4)$$

The parameters eQq_0 and eQq_2 are the ^{197}Au diagonal and off-diagonal electric quadrupole coupling constants. For the present case of the [17.7] $\Omega = 1$ state, the value of Ω in eqs 3 and 4 was set to 1.

For the $X^1\Sigma^+$ state, hyperfine structure arises only from the ^{197}Au electric quadrupole interaction and from nuclear spin-rotation coupling. The matrix elements were written as[13]

$$\begin{aligned}\langle {}^1\Sigma; JI_1F_1I_2F|\mathbf{H}_{\text{mag}}|{}^1\Sigma; J'I_1F'_1I_2F\rangle = &c_I^{(1)}(-1)^{J+I_1+F_1}[J(J+1)(2J+1)]^{1/2} \times \\ &[I_1(I_1+1)(2I_1+1)]^{1/2}\begin{Bmatrix} I_1 & J & F_1 \\ J & I_1 & 1\end{Bmatrix}\delta_{JJ'}\delta_{F_1F'_1} + \\ &c_I^{(2)}(-1)^{J+I_1+I_2+2F_1+F+1}[J(J+1)(2J+1)]^{1/2} \times \\ &[I_2(I_2+1)(2I_2+1)]^{1/2}[(2F_1+1)(2F'_1+1)]^{1/2} \times \\ &\begin{Bmatrix} F'_1 & J' & I_1 \\ J & F_1 & 1\end{Bmatrix}\begin{Bmatrix} I_2 & F'_1 & F \\ F_1 & I_2 & 1\end{Bmatrix}\delta_{JJ'}\end{aligned} \quad (5)$$

$$\begin{aligned}\langle {}^1\Sigma; JI_1F_1I_2F|\mathbf{H}_{\text{elec}}|{}^1\Sigma; J'I_1F'_1I_2F\rangle = &\frac{1}{4}eQq_0^{(1)}(-1)^{J+J'+I_1+F_1}[(2J+1)(2J'+1)]^{1/2}\begin{pmatrix} J' & 2 & J \\ 0 & 0 & 0\end{pmatrix} \times \\ &\begin{Bmatrix} I_1 & J' & F_1 \\ J & I_1 & 2\end{Bmatrix}\begin{pmatrix} I_1 & 2 & I_1 \\ -I_1 & 0 & I_1\end{pmatrix}^{-1}\delta_{F_1F'_1}\end{aligned} \quad (6)$$

Here $c_I^{(1)}$ and $c_I^{(2)}$ are the ^{197}Au and ^{19}F nuclear spin-rotation coupling constants, respectively.

From the outset, it was clear that the hyperfine structure of the band is dominated by the ^{197}Au magnetic hyperfine interaction in the upper state. The hyperfine splittings appear as Landé patterns, corresponding to magnetic hyperfine structure rather than electric quadrupole structure. The ^{19}F hyperfine splittings in the upper state are nearly an order of magnitude smaller than those of ^{197}Au. The ground-state hyperfine splittings are much smaller still. Because the ^{19}F hyperfine interaction is much smaller than the ^{197}Au interaction in both electronic states, F_1 is nearly a good quantum number. In this limit, the relative intensity, S, of each hyperfine component in a particular rotational line is given by the formula[14]

$$S(J'I_1F'_1I_2F' \leftarrow JI_1F_1I_2F) = (2F_1+1)(2F'_1+1) \times (2F+1)(2F'+1)\begin{Bmatrix} J' & F'_1 & I_1 \\ F_1 & J & 1\end{Bmatrix}^2\begin{Bmatrix} F'_1 & F' & I_2 \\ F & F'_1 & 1\end{Bmatrix}^2 \quad (7)$$

For transitions with $J'' \geq 4$, only the eight "main" $\Delta F = \Delta F_1 = \Delta J$ hyperfine components were observed, and the F and F_1 quantum numbers could easily be assigned by their relative intensities. For the first few members of each rotational branch, however, we also observed many blended $\Delta F \neq \Delta J$ or $\Delta F_1 \neq \Delta J$ hyperfine "satellite" transitions. A good example of this behavior is shown in Figure 2, which displays the sub-Doppler spectrum of the first two Q lines. After preliminarily fitting the lines where only the main components were observed, we could make accurate predictions for the wavenumbers of all possible hyperfine components of the low-J lines. With relative intensities calculated from eq 7, we were then able to assign the various hyperfine components of these lines securely. The energy level diagram shown in Figure 2 displays the hyperfine splittings in the two rotational levels involved in each transition, as calculated from the final values of the molecular constants. We have indicated the assigned hyperfine components using vertical tie lines in the diagram, with thicker lines denoting stronger components. For clarity, the ground state ^{197}Au splitting is exaggerated by a factor of 10, whereas the ^{19}F ground state splitting is 3 orders of magnitude smaller still and is not shown.

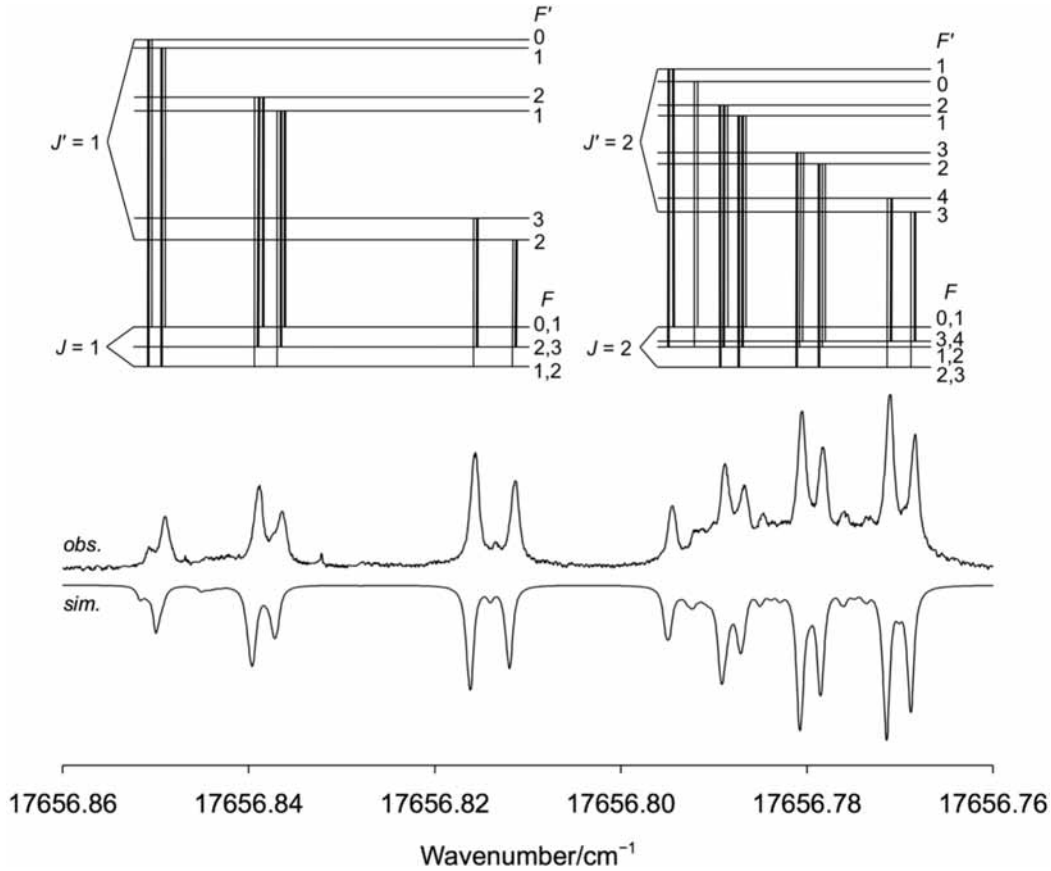

Figure 2. Sub-Doppler spectrum of the first two Q lines [$Q(1)$ and $Q(2)$] of the [17.7]1$-X^1\Sigma^+$ (0,0) band of AuF recorded by intermodulated fluorescence spectroscopy. The relative energies of the hyperfine levels involved in this transition are shown above the spectrum with tie lines identifying the individual components. The values of J and F are given, and the values of F_1 can be determined by inspection. The upper trace is the observed spectrum; the lower trace is a simulated spectrum using calculated transition wavenumbers and intensities.

It is clear from this diagram that there are many blended hyperfine components created by the small size of the hyperfine splittings of the lower level. Whereas this ground-state hyperfine structure was resolvable in the microwave work,[3] we were not able to resolve it in the optical region.

The sub-Doppler spectra of the lowest-J transitions are further blended by crossover resonances, which are experimental artifacts of the intermodulated fluorescence (IMF) technique.[9] The frequency ν_C of the crossover resonance is the arithmetic mean of the two parent frequencies, $\nu_C = (1/2)(\nu_1 + \nu_2)$, whereas its intensity S_C is proportional to the geometric mean of the two parent intensities, $S_C \propto (S_1S_2)^{1/2}$.[9,15] To demonstrate that our hyperfine assignments are correct, we generated a synthetic spectrum of the $Q(1)$ and $Q(2)$ transitions, which is reproduced below the experimental spectrum in Figure 2. This synthetic spectrum includes both parent and crossover resonances. We calculated the intensity of each crossover resonance using the equation

$$S_C = f_C(S_1S_2)^{1/2} \exp\left\{-2(\ln 2)\left(\frac{\Delta\nu}{2\alpha_G}\right)^2\right\} \qquad (8)$$

where α_G is the Gaussian (Doppler) line width (HWHM) of the two parent transitions and f_C is a proportionality constant that is a function of the lifetimes of the coupled states and which is always <2.[15] We calculated Lorentzian lineshapes for all 56 allowed transitions in the $Q(1)$ and $Q(2)$ lines and their 184 crossover resonances, using eq 8 for the crossover intensities. We varied the two line width parameters and the proportionality constant, f_C, iteratively to provide the best agreement between the observed and simulated spectrum. In the final simulation shown in Figure 2, we used a Lorentzian HWHM line width of 12 MHz, a Gaussian HWHM line width of 220 MHz (which corresponds to a translational temperature of 300 K), and a proportionality constant $f_C = 0.4$.

Crossover resonances arising from transitions coupled to a common upper level fall nearly on top of their parent transitions because the hyperfine splittings in the lower state are smaller than the Lorentzian line width of the sub-Doppler transitions. These have the effect of slightly broadening the observed transitions. Coupled transitions from a common lower level are separated by the upper state hyperfine splittings, which generally placed their crossover resonances at a frequency away from any other parent transitions. Several of these lower-level crossover resonances can be seen in Figure 2, particularly between the strong pairs of parent transitions in the $Q(2)$ line. The simulated spectrum reproduces these experimental features quite well. The strength of satellite transitions calculated using eq 7 dies off approximately as $1/J^2$ so that for transitions with $J'' \geq 4$, we assigned the observed hyperfine components as arising only from main transitions.

Using our parametrized Hamiltonian, we fitted data from the 16 lines for which we were able to resolve the hyperfine structure in our sub-Doppler spectra. Each datum was weighted by the inverse square of its estimated uncertainty. We included in our fit the microwave measurements of the $J'' = 1-0$ transition.[3] These measurements are of much higher resolution than our optical data and essentially completely determine the value of the ground-state hyperfine parameters in our fit. We

TABLE 1: Observed Wavenumbers of the [17.7]1−$X^1\Sigma^+$ (0,0) Band of AuF Recorded at Sub-Doppler Resolution[a]

branch	$F''-F_1''$	ΔF	ΔF_1	$F_1'' = J'' + 1.5$	$F_1'' = J'' + 0.5$	$F_1'' = J'' - 0.5$	$F_1'' = J'' - 1.5$
R(0)	0.5	1	1	^{17}657.3160(−7)			
	−0.5	1	1	657.3117(−8)			
	0.5	0	0	657.3398(−6)			
	−0.5	0	0	657.3372(−7)			
	0.5	−1	−1	657.3500(−2)			
	−0.5	−1	−1	657.3517(−1)			
R(1)	0.5	1	1	657.7844(−19)*	^{17}657.7941(−17)*	^{17}657.8020(−15)*	
	−0.5	1	1	657.7817(−20)*	657.7918(−18)*	657.7992(−23)*	
	0.5	0	0	657.7941(−12)*	657.8027(−16)*	657.8086(−10)*	
	−0.5	0	0	657.7918(−13)*	657.8008(−15)*		
	−0.5	1	0			657.8086(−10)*	
R(2)	0.5	1	1	658.2217(−6)	658.2265(−7)	658.2327(−6)*	^{17}658.2386(−5)*
	−0.5	1	1	658.2198(−6)	658.2248(−7)	658.2311(−6)*	658.2368(−5)*
	0.5	0	0		658.2327(−9)*	658.2386(−10)*	
	−0.5	0	0		658.2311(−9)*		
R(3)	0.5	1	1	658.6273(9)	658.6301(10)	658.6351(11)*	658.6409(14)*
	−0.5	1	1	658.6259(10)	658.6286(9)	658.6338(12)*	658.6395(14)*
	0.5	0	0		658.6351(9)*	658.6409(9)*	
	−0.5	0	0		658.6338(10)*		
R(4)	0.5	1	1	658.9983(−6)*	658.9993(−11)	659.0033(−11)	659.0086(−11)
	−0.5	1	1	658.9971(−6)	658.9983(−9)*	659.0024(−9)	659.0076(−9)
Q(1)	0.5	0	0	656.7957(−4)*	656.8189(−13)*	656.8290(−2)*	
	−0.5	0	0	656.7913(−6)*	656.8164(−13)*		
	0.5	1	1		656.7957(−8)	656.8189(−8)*	
	−0.5	1	1		656.7913(−10)*		
	0.5	−1	−1	656.8189(−5)*	656.8290(−10)*		
	−0.5	−1	−1	656.8164(−9)*	656.8307(−10)*		
	0.5	0	1			656.8164(−5)*	
	−0.5	1	1			656.8164(−5)*	
Q(2)	0.5	0	0	656.7511(−3)*	656.7605(−4)*	656.7688(−3)*	656.7745(−2)*
	−0.5	0	0	656.7484(−4)*	656.7583(−4)*	656.7668(−3)*	
	0.5	1	1			656.7605(−1)*	
	−0.5	1	1			656.7583(−1)*	
	0.5	−1	−1	656.7605(0)*	656.7688(−6)*	656.7745(−7)*	
	−0.5	−1	−1	656.7583(0)*	656.7668(−6)*		
Q(3)	0.5	0	0	656.6797(2)	656.6846(2)*	656.6907(1)*	656.6963(−1)*
	−0.5	0	0	656.6777(1)	656.6828(2)*	656.6891(2)*	656.6946(0)*
Q(4)	0.5	0	0	656.5824(5)	656.5854(8)	656.5903(8)	656.5958(7)
	−0.5	0	0	656.5809(5)	656.5839(7)	656.5889(8)	656.5943(7)
Q(5)	0.5	0	0	656.4583(−7)*	656.4598(−7)	656.4638(−7)	656.4690(−8)
	−0.5	0	0	656.4570(−8)	656.4583(−10)*	656.4624(−10)	656.4678(−9)
Q(6)	0.5	0	0	656.3105(−6)*	656.3113(−5)*	656.3156(4)	656.3206(3)
	−0.5	0	0	656.3096(−5)*	656.3105(−3)*	656.3148(5)	656.3198(5)
P(2)	0.5	−1	−1	655.7363(2)*	655.7601(−1)*	655.7696(−1)*	
	−0.5	−1	−1	655.7320(0)*	655.7575(−3)*	655.7714(0)*	
	0.5	0	0		655.7363(−3)*	655.7601(2)*	655.7696(3)*
	−0.5	0	0		655.7320(−4)*	655.7575(1)*	
	−0.5	−1	0				655.7714(4)*
	−0.5	1	0				655.7696(3)*
P(3)	0.5	−1	−1	655.1527(6)*	655.1622(6)*	655.1705(6)*	655.1763(7)*
	−0.5	−1	−1	655.1500(5)*	655.1599(4)*	655.1685(5)*	655.1739(6)*
P(4)	0.5	−1	−1	654.5357(11)	654.5405(10)	654.5467(9)	654.5524(8)
	−0.5	−1	−1	654.5338(10)	654.5388(10)	654.5450(9)	654.5507(9)
P(5)	0.5	−1	−1	653.8862(10)	653.8888(9)	653.8937(9)	653.8992(8)
	−0.5	−1	−1	653.8848(11)	653.8874(9)	653.8924(9)	653.8978(8)
P(6)	0.5	−1	−1	653.2039(−3)*	653.2051(−5)	653.2091(−6)	653.2144(−6)
	−0.5	−1	−1	653.2026(−4)	653.2039(−6)*	653.2080(−6)	653.2133(−6)

[a] Values in parentheses are residuals in units of the last reported digit. Asterisks indicate blended or very weak lines that were deweighted in the least-squares fit.

did not include the higher-J, pure rotational transitions reported in ref 4 because the hyperfine structure was not resolved in those measurements. In Table 1, we report the transition wavenumbers and least-squares fit residuals for all of the observed hyperfine components. In Table 2, we report the molecular constants derived from this fit. For the ground state, we compare these constants with those determined in the microwave work,[3] and it can be seen that the two are in excellent agreement. The hyperfine Hamiltonians used in the present work and that of ref 3 are identical, and the fitted constants (as well as the residuals for the microwave transitions) are essentially identical. Our value for the rotational constant is slightly different owing to the fact that we have included the centrifugal distortion terms D and H, fixed at the values determined by fitting our Doppler-limited spectrum. In the microwave experiment, only the $J = 1-0$ transition was measured, so that its wavenumber was taken to be $\tilde{\nu}_{J=1-0} = 2B_{\text{eff}}$, whereas in our work $\tilde{\nu}_{J=1-0} = 2B - 4D + 8H$. Using our fitted constants, we find $B_{\text{eff}} = 0.263409550(21)$

TABLE 2: Molecular Constants (in inverse centimeters) for the [17.7]1 ($v = 0$) and $X^1\Sigma^+$ ($v = 0$) States of AuF[a]

constant	this work	microwave (ref 3)
	$X^1\Sigma^+$ ($v = 0$)	
B	0.263410015(21)	0.263409554(16)
D	[2.3237×10^{-7}]	
H	[-1.15×10^{-13}]	
c_I (^{197}Au)	$-2.62\ (27) \times 10^{-7}$	$-2.62\ (17) \times 10^{-7}$
c_I (^{19}F)	$-4.57\ (92) \times 10^{-7}$	$-5.50\ (57) \times 10^{-7}$
eQq_0 (^{197}Au)	−0.00177571(27)	−0.00177571(22)
	[17.7]1 ($v = 0$)	
T_0	17 656.83350(13)	
B	0.2494601(59)	
D	[1.8996×10^{-7}]	
H	[-1.92×10^{-12}]	
q	−0.0031334(63)	
q_D	[-9.33×10^{-8}]	
q_H	[3.78×10^{-12}]	
h_1 (^{197}Au)	−0.01812(15)	
h_1 (^{19}F)	0.00665(45)	
eQq_0 (^{197}Au)	−0.01347(63)	

[a] Values in parentheses represent one standard deviation in units of the last quoted digit. Constants in brackets were fixed at these values, taken from a least-squares fit to higher-J Doppler-limited data.

cm^{-1}, which agrees closely with the microwave value of $B_{eff} =$ 0.263409554(16) cm^{-1}.

In one stage in the least-squares fitting, we tried determining the parity-dependent, off-diagonal electric quadrupole constant eQq_2 (^{197}Au) in the upper state. However, the fitted parameter's uncertainty was greater than its magnitude, indicating that the data were insensitive to this parameter; in the final least-squares fit, it was set to zero.

Discussion

Magnetic hyperfine structure can be used to probe the electronic structure of a diatomic molecule, a consequence of the fact that the hyperfine parameters are proportional to certain expectation values of the molecule's unpaired electrons. In this way, hyperfine structure can yield direct information about the molecular wave function. This is particularly true in the present situation, where the sign of the ^{197}Au magnetic hyperfine parameter h_1 reflects the character of the upper state.

It is instructive to begin by considering the results of the ab initio calculation by Guichemerre et al.,[6] who employed multireference configuration interaction (MRCI) and coupled-cluster (CC) methods with scalar relativistic energy-consistent pseudopotentials. These workers found that the ground and lowest excited electronic states of AuF are well described by the electronic configurations

$$X^1\Sigma^+:(1\sigma)^2(1\pi)^4(1\delta)^4(2\pi)^4(2\sigma)^2 \quad (9)$$

$$^{1,3}\Sigma^+:(1\sigma)^2(1\pi)^4(1\delta)^4(2\pi)^4(2\sigma)^1(3\sigma)^1 \quad (10)$$

$$^{1,3}\Pi:(1\sigma)^2(1\pi)^4(1\delta)^4(2\pi)^3(2\sigma)^2(3\sigma)^1 \quad (11)$$

$$^{1,3}\Delta:(1\sigma)^2(1\pi)^4(1\delta)^3(2\pi)^4(2\sigma)^2(3\sigma)^1 \quad (12)$$

where the 1σ and 1π orbitals are derived mostly from F 2p atomic orbitals (AOs), the 1δ orbitals are Au 5dδ AOs, the 2π orbitals are antibonding combinations of Au 5dπ and F 2pπ AOs, the 2σ orbital is an Au 5dσ AO, and the 3σ orbital is an Au 6s AO. Therefore, electronic transitions out of the AuF ground state correspond largely to a 5d → 6s transition on the gold atom, with the orbital symmetry (Λ) of the upper state determined by whether the electron being excited originates from a 5d σ, π, or δ orbital. Such metal-centered d → s transitions should be relatively weak, although the $^{1,3}\Pi$ states will gain intensity from the partial fluorine-to-gold charge transfer that occurs upon excitation from a 2π molecular orbital to 3σ.

From the observations of first lines in the rotational branches, we can definitively assign the upper state as $\Omega = 1$. In a Hund's case a basis, restricting ourselves to singlet and triplet states, there are four possible states that can produce an $\Omega = 1$ component: $^3\Sigma$, $^1\Pi$, $^3\Pi$, and $^3\Delta$. The ab initio calculation[6] predicts that one of each of these four states exists below 4 eV in energy. We expect that these four $\Omega = 1$ components, $^3\Sigma_1$, $^1\Pi_1$, $^3\Pi_1$, and $^3\Delta_1$, will be appreciably mixed by the large gold spin−orbit interaction, which acts between states of the same Ω. Therefore, the molecular eigenstates will make a transition to Hund's case c, where Λ, S, and Σ are mixed, leaving Ω as the only good quantum number.

We now consider the form of the diagonal magnetic hyperfine matrix elements for the ^{197}Au nucleus (I_1). The hyperfine Hamiltonian for a linear molecule in a Hund's case a basis was first described by Frosch and Foley.[16] We follow their formulation, except that we prefer to use the Fermi contact parameter b_F in place of their parameter b because b_F has a more direct physical interpretation. The two parameters are related as $b_F = b + (1/3)c$. The diagonal ^{197}Au matrix elements of this Hamiltonian are as follows

$$\langle \Lambda S\Sigma; J\Omega I_1F_1I_2F|\mathbf{H}^{(1)}_{\text{mag hfs}}|\Lambda S\Sigma; J\Omega I_1F_1I_2F\rangle = \left[a\Lambda + \left(b_F + \frac{2}{3}c\right)\Sigma\right]\Omega\left[\frac{F_1(F_1+1) - I_1(I_1+1) - J(J+1)}{2J(J+1)}\right] \quad (13)$$

where for simplicity, we have dropped the superscript (1) on these ^{197}Au hyperfine parameters. We are neglecting here the parity-dependent term (d) that acts between the $\Lambda = \pm 1$ components of a Π state. This term produces different hyperfine structure in the two parity components. Its effects are realized if the P, R-branch hyperfine splittings cannot be fitted together with the Q-branch splittings using the same formula, but we observed no such parity asymmetry in our spectrum.

The magnetic hyperfine structure in an electronic state will order itself according to the sign of the quantity $h_\Omega \cdot \Omega$ in a manner analogous to spin−orbit fine structure: if $h_\Omega \cdot \Omega > 0$, then a "regular" Landé pattern will form with levels of higher F_1 lying to higher energy, whereas if $h_\Omega \cdot \Omega < 0$, then an "inverted" pattern is formed. In the present case of AuF, the pattern is inverted, implying that the quantity $h_\Omega \cdot \Omega$ is negative. This result is in sharp contrast with the upper ($b^3\Pi$) state of the yellow bands of CuF, which forms a regular metal hyperfine pattern,[8,12] ruling out the possibility that the upper states of the yellow systems of CuF and AuF are analogous.

We evaluate the magnetic hyperfine parameter in Table 3 for the four singlet or triplet states that produce $\Omega = 1$ components. The values of h_Ω shown in this table are for the $\Omega = +1$ component in a signed-Ω basis; for the $\Omega = -1$ component, h_Ω will have the opposite sign, but the product $h_\Omega \cdot \Omega$ will have the same sign.

TABLE 3: Value of the Magnetic Hyperfine Parameter, h_Ω, for $\Omega = 1$ Components of Hund's Case (a) States

state	value of h_Ω
$^3\Sigma_1$	$b_F + 2/3c$
$^1\Pi_1$	a
$^3\Pi_1$	a
$^3\Delta_1$	$2a - b_F - 2/3c$

The case a hyperfine parameters a, b_F, and c can be expressed in terms of the wave functions of the valence electrons as follows[17]

$$a = 2\mu_B g_N \mu_N \sum_i \left\langle \frac{1}{r_i^3} \right\rangle \tag{14}$$

$$b_F = \left(\frac{8\pi}{3}\right) g \mu_B g_N \mu_N \left(\frac{1}{2S}\right) \sum_i |\langle \psi_i(r_i = 0)\rangle|^2 \tag{15}$$

$$c = \left(\frac{3}{2}\right) g \mu_B g_N \mu_N \left(\frac{1}{2S}\right) \sum_i \left\langle \frac{3\cos^2\theta_i - 1}{r_i^3} \right\rangle \tag{16}$$

where μ_B and μ_N are the Bohr and nuclear magnetons, g and g_N are the electron and nuclear g factors, and r_i and θ_i are the spherical polar coordinates of the valence electrons over which the summation is taken. For the electron orbital−nuclear spin coupling constant a, only electrons with $\lambda \neq 0$ contribute; for the Fermi contact interaction, b_F, and the electron spin−nuclear spin dipolar coupling constant, c, only unpaired electrons are included. Multiplying each of these equations on the right by the factor $10^{-6}\mu_0/4\pi h$ ($= 10^{-13}/h$) expresses each parameter as a frequency in units of megahertz.

The nuclear g factor for ^{197}Au is positive, $g_N = \mu_I/I = 0.098772$,[18] which means that the factors in front of the summations in eqs 14−16 are all positive. Therefore, the parameters a and b_F must be positive because the summations in eqs 14 and 15 are necessarily positive. The sign of the dipolar parameter c (eq 16) depends on the relative contributions of the unpaired electrons in the summation through the signs and magnitudes of the angular integrals $\langle 3\cos^2\theta_i - 1\rangle$. In light of these observations, we can see immediately from Table 3 that if the upper state in our transition was only $^3\Pi_1$ or $^1\Pi_1$ in character, then we would predict a positive value for the hyperfine constant, $h_1 = a > 0$. If the upper state was $\cdots(2\sigma)^1(3\sigma)^1\ ^3\Sigma^+$, then we would also predict a positive value for $h_1 = b_F + (2/3)c$ because b_F is positive and the 2σ and 3σ contributions to c are positive and zero, respectively. (The integral $\langle 3\cos^2\theta - 1\rangle$ is $+4/7$ for dσ and 0 for sσ.).[17] The only case a $\Omega = 1$ component that can lead to a negative value of h_1 is $^3\Delta_1$, for which $h_1 = 2a - b_F - (2/3)c$.

The value of h_1 for a pure $^3\Delta_1$ state of AuF described by eq 12 can now be estimated in the following manner. The two unpaired electrons in this state are in Au δ_{5d} and σ_{6s} atomic orbitals. Only the Au δ_{5d} electron will contribute to the parameters a and c. Its contribution can be approximated using the results of a Hartree−Fock self-consistent field calculation on the gold atom: $\langle r^{-3}\rangle_{5d} = 13.426a_0^{-3}$ for the Au $5d^96s6p$ configuration and $\langle r^{-3}\rangle_{5d} = 14.359a_0^{-3}$ for the Au^+ $5d^86s6p$ configuration.[19] In the $^3\Delta_1$ state of AuF, the neutral configuration is more relevant because it contains nine 5d electrons. Using this value for $\langle r^{-3}\rangle_{5d}$ in eq 14, we predict a value of $a = 126.5$ MHz ($^3\Delta$). Together with the value $\langle 3\cos^2\theta - 1\rangle_{d\delta} = -4/7$,[17] we also predict from eq 16 a value of $c = -54.2$ MHz ($^3\Delta$). Finally, to estimate the molecular Fermi contact parameter, b_F, we can use the Au atomic hyperfine splitting measured in the ground $(5d^{10}6s^1)\ ^2S_{1/2}$ state. Because the dipolar term in this atomic state is zero, the splitting is due only to the Fermi contact interaction and provides the value $A = b_F(Au) = 3049.7$ MHz.[20] This result yields $b_F(AuF) = (1/2)b_F(Au) = 1524.8$ MHz ($^3\Delta$). With these estimated values, we predict that $h_1 = 2a - b_F - (2/3)c = -1235.6$ MHz ($^3\Delta_1$). The fitted value for this parameter (Table 2) is $-543(4)$ MHz, so it seems clear that the [17.7]1 state is not pure $^3\Delta_1$. Of the three other $\Omega = 1$ states in the same energy region, $^3\Sigma_1$, $^1\Pi_1$, and $^3\Pi_1$,[6] it is only the $^1\Pi_1$ state that provides electric dipole transition intensity to the ground state. If we momentarily write the upper state as a mixture of only these two states, $|[17.7]1\rangle = \alpha|^3\Delta_1\rangle + \beta|^1\Pi_1\rangle$, then

$$\langle [17.7]1|\mathbf{H}_{mag\ hfs}|[17.7]1\rangle = \alpha^2\langle ^3\Delta_1|\mathbf{H}_{mag\ hfs}|^3\Delta_1\rangle + \beta^2\langle ^1\Pi_1|\mathbf{H}_{mag\ hfs}|^1\Pi_1\rangle + 2\alpha\beta\langle ^3\Delta_1|\mathbf{H}_{mag\ hfs}|^1\Pi_1\rangle \tag{17}$$

Following eq 13, this produces a diagonal ^{197}Au magnetic hyperfine matrix element of

$$\langle [17.7]1|\mathbf{H}_{mag\ hfs}|[17.7]1\rangle_{diag} = [\alpha^2 h_1(^3\Delta_1) + \beta^2 h_1(^1\Pi_1)]\Omega\left[\frac{F_1(F_1+1) - I_1(I_1+1) - J(J+1)}{2J(J+1)}\right] \tag{18}$$

because the hyperfine cross-term in eq 17 is zero. Simultaneously solving the equations

$$\alpha^2 + \beta^2 = 1 \tag{19}$$

and

$$\alpha^2 h_1(^3\Delta_1) + \beta^2 h_1(^1\Pi_1) = \alpha^2\left(2a - b_F - \frac{2}{3}c\right) + \beta^2(a) \approx \alpha^2(-1235.6\ \text{MHz}) + \beta^2(126.5\ \text{MHz}) = -543.2\ \text{MHz} \tag{20}$$

yields $\alpha^2 = 0.49$ and $\beta^2 = 0.51$. We recognize that this semiquantitative model neglects mixing with $^3\Sigma_1$ and $^3\Pi_1$ states; with only one measured ^{197}Au magnetic hyperfine parameter, there is not enough information to assess the degree of this mixing. We do note, however, that the ab initio MRCI-CC calculation[6] places the $^1\Pi$ state only 1800 cm^{-1} below the $^3\Delta$ state, with the $^3\Pi$ and $^3\Sigma^+$ states located 6500 and 10 000 cm^{-1} below $^3\Delta$, respectively.

Furthermore, we can estimate the size of the spin−orbit matrix element between the $^1\Pi$ and $^3\Delta$ states. Assuming that each state belongs to the single configurations described by the ab initio calculation, $\cdots\delta^4\pi^3\sigma$, $^1\Pi$ and $\cdots\delta^3\pi^4\sigma$, $^3\Delta$ (eqs 11 and 13), then we can write Slater determinantal wave functions for the two $\Omega = 1$ components as follows[21]

$$^1\Pi_1: \frac{1}{\sqrt{2}}|\delta^+\alpha\delta^+\beta\delta^-\alpha\delta^-\beta\pi^+\alpha\pi^+\beta\pi^-\alpha\sigma\beta| - \frac{1}{\sqrt{2}}|\delta^+\alpha\delta^+\beta\delta^-\alpha\delta^-\beta\pi^+\alpha\pi^+\beta\pi^-\beta\sigma\alpha| \tag{21}$$

$$^3\Delta_1:|\delta^+\alpha\delta^+\beta\delta^-\beta\pi^+\alpha\pi^+\beta\pi^-\alpha\pi^-\beta\sigma\beta| \quad (22)$$

The spin−orbit matrix element between these $\Omega = 1$ components is evaluated as

$$\langle ^1\Pi_1, v|\mathbf{H}_{s.o.}|^3\Delta_1, v'\rangle = \left\langle ^1\Pi_1, v\left|\frac{1}{2}\sum_{i=1}^{8}\hat{a}_i(\mathbf{l}_i^+\mathbf{s}_i^- + \mathbf{l}_i^-\mathbf{s}_i^+)\right|^3\Delta_1, v'\right\rangle$$

$$= \frac{1}{\sqrt{2}}\cdot\frac{1}{2}\langle\delta^-|\hat{a}\mathbf{l}^-|\pi^-\rangle\langle v|v'\rangle$$

$$= \frac{1}{4}\sqrt{2}a_+\langle v|v'\rangle \quad (23)$$

where $a_+ = \langle\delta^-|\hat{a}\mathbf{l}^-|\pi^-\rangle = \langle\pi^-|\hat{a}\mathbf{l}^+|\delta^-\rangle$. The molecular spin−orbit matrix element, a_+, can be related to the atomic spin−orbit constant, ζ, by recognizing that $\mathbf{l}^+|d\delta^-\rangle = (l(l+1) - \lambda(\lambda+1))^{1/2}|d\pi^-\rangle = 2|d\pi^-\rangle$ so that $a_+ = \langle\pi^-|\hat{a}\mathbf{l}^+|\delta^-\rangle = 2\zeta_{Au}(5d)$. Using the value $\zeta_{Au}(5d) = 5097\ cm^{-1}$ from ref 21, we find $\langle ^1\Pi_1,v|\mathbf{H}_{s.o.}|^3\Delta_1,v'\rangle \approx (3600\ cm^{-1})\cdot\langle v|v'\rangle$. With spin−orbit matrix elements this large, the mixing of these two states will be substantial, which supports our analysis of the ^{197}Au magnetic hyperfine structure. To summarize, the negative sign of the ^{197}Au magnetic hyperfine constant h_1 can be rationalized by assuming that the upper state in the transition has significant $^3\Delta_1$ character. The transition intensity to the ground state can be accounted for by spin−orbit mixing of this state with the nearby $^1\Pi_1$ state.

Guichemerre et al.[6] also performed an ab initio calculation on AuF that took account of the spin−orbit interactions. Largely on the basis of the calculated term energies, they assigned the two upper states in the yellow region (our [17.8]0 and [17.7]1 states) as those with leading character $^3\Pi_0$ and $^3\Pi_1$, which they calculated to lie at 19 360 and 18 870 cm^{-1}, respectively. We prefer to assign the [17.8]0 and [17.7]1 states as those with leading character $^1\Sigma_0^+$ and $^1\Pi_1$, which were calculated to lie at 28 870 and 28 550 cm^{-1},[6] with the $^1\Pi_1$ state heavily mixed with $^3\Delta_1$, as we have just shown. We also intend to record higher resolution spectra of the (1,0) and (0,0) bands of the [14.3]1−$X^1\Sigma^+$ system, which lie at 688 and 715 nm. These red bands are considerably weaker than the yellow bands, suggesting an assignment of the [14.3]1 state as the $^3\Pi_1$ state located in the ab initio calculation at 18 870 cm^{-1}, because a $^3\Pi_1$−$^1\Sigma$ transition would be weaker than a $^1\Pi_1$−$^1\Sigma$ transition. The only other $\Omega = 1$ state calculated to lie in this region is a $^3\Sigma^+$ state at 14 300 cm^{-1}, but the rotational structure of the red bands is not consistent with a $^3\Sigma_1$−$^1\Sigma$ assignment. To summarize, the present spectroscopic characterization of the low-lying electronic states of AuF is not in good agreement with the ab initio predictions.

Finally, we note that the sign of the ^{19}F magnetic hyperfine constant, $h_1 = 199(13)$ MHz, is positive. This constant arises from the interaction of the gold-centered unpaired electrons with the ^{19}F nucleus located one bond length away. Because the nuclear g factor for ^{19}F is positive, we expect that the case a hyperfine constants a and c will both be positive and of comparable size. To first order, the ^{19}F Fermi contact interaction constant b_F is zero because there are no unpaired fluorine-centered electrons in AuF. However, spin polarization of the σ_{F2s} orbital could produce a small Fermi contact term, the magnitude of which is difficult to calculate. With these points in mind, it is not surprising that h_1 is positive because the term $h_1 = \alpha^2(2a - b_F - (2/3)c) + \beta^2(a)$ for the ^{19}F nucleus is likely to be positive.

Conclusions

The AuF [17.7]1−$X^1\Sigma^+$ (0,0) band at 566 nm has been recorded by laser excitation spectroscopy using a hollow cathode discharge source. An analysis of both the Doppler-limited and sub-Doppler spectrum has yielded values for the upper state rotational, Ω-doubling, and ^{197}Au and ^{19}F hyperfine constants for the first time. It has been shown that the sign and magnitude of the ^{197}Au magnetic hyperfine constant of the [17.7]1 state is consistent with the state having significant $^3\Delta_1$ character, where large spin−orbit mixing with a nearby $^1\Pi_1$ state would provide electric dipole transition intensity to the ground electronic state. This finding demonstrates the utility of hyperfine interactions in determining the character of molecular electronic states.

Acknowledgment. This work has been supported by the National Science Foundation under grant nos. CHE-0518198 and CHE-0812878. We acknowledge the Donors of the American Chemical Society Petroleum Research Fund for partial support of this research. We thank Kara Manke and Tyson Vervoort for their help in recording low-resolution spectra of AuF. It is a pleasure to dedicate this paper in honor of Professor Robert W. Field, whose tremendous insight into the electronic structure and spectroscopy of diatomic molecules has influenced the work presented here.

References and Notes

(1) Saenger, K. L.; Sun, C. P. *Phys. Rev. A* **1992**, *46*, 670.
(2) Andreev, S.; BelBruno, J. J. *Chem. Phys. Lett.* **2000**, *329*, 490.
(3) Evans, C. J.; Gerry, M. C. L. *J. Am. Chem. Soc.* **2000**, *122*, 1560.
(4) Okabayashi, T.; Nakaoka, Y.; Yamazaki, E.; Tanimoto, M. *Chem. Phys. Lett.* **2002**, *366*, 406.
(5) Schwerdtfeger, P.; McFeaters, J. S.; Stephens, R. L.; Liddell, M. J.; Dolg, M.; Hess, B. A. *Chem. Phys. Lett.* **1994**, *218*, 362.
(6) Guichemerre, M.; Chambaud, G.; Stoll, H. *Chem. Phys.* **2002**, *280*, 71.
(7) Linton, C.; Dulick, M.; Field, R. W.; Carette, P.; Leyland, P. C.; Barrow, R. F. *J. Mol. Spectrosc.* **1983**, *102*, 441.
(8) Steimle, T. C.; Brazier, C. R.; Brown, J. M. *J. Mol. Spectrosc.* **1982**, *91*, 137.
(9) Demtröder, W. *Laser Spectroscopy*, 3rd ed.; Springer-Verlag: Berlin, 2003.
(10) Bernath, P. F. *Spectra of Atoms and Molecules*, 2nd ed.; Oxford University Press: Oxford, U.K., 2005.
(11) Brown, J. M.; Carrington, A. *Rotational Spectroscopy of Diatomic Molecules*; Cambridge University Press: Cambridge, U.K., 2003.
(12) Steimle, T. C.; Brazier, C. R.; Brown, J. M. *J. Mol. Spectrosc.* **1985**, *110*, 39.
(13) Ryzlewicz, C.; Schutze-Pahlmann, H. U.; Hoeft, J.; Torring, T. *Chem. Phys.* **1982**, *71*, 389.
(14) Gordy, W.; Cook, R. L. *Microwave Molecular Spectra*, 3rd ed.; John Wiley & Sons: New York, 1984; eq 15.147.
(15) Sorem, M. S.; Hänsch, T. W.; Schawlow, A. L. *Chem. Phys. Lett.* **1972**, *17*, 300.
(16) Frosch, R. A.; Foley, H. M. *Phys. Rev.* **1952**, *88*, 1337.
(17) Varberg, T. D.; Field, R. W.; Merer, A. J. *J. Chem. Phys.* **1991**, *95*, 1563.
(18) I. Mills, I.; Cvitas, T.; Homann, K.; Kallay, N.; Kuchitsu, K. *Quantities, Units and Symbols in Physical Chemistry*, 2nd ed.; Blackwell: Oxford, U.K., 1993.
(19) Esquivel, D. M. S.; Guenzburger, D.; Danon, J. *Phys. Rev. B* **1979**, *19*, 1357.
(20) Dahmen, H.; Penselin, S. *Z. Phys.* **1967**, *200*, 456.
(21) Lefebvre-Brion, H.; Field, R. W. *The Spectra and Dynamics of Diatomic Molecules*; Elsevier: Amsterdam, 2004.

JP904472Y